ADVANCED FUNCTIONAL MATERIALS
www.afm-journal.de

Flexible Organic Photovoltaic Cells with In Situ Nonthermal Photoreduction of Spin-Coated Graphene Oxide Electrodes

Emmanuel Kymakis, Kyriaki Savva, Minas M. Stylianakis, Costas Fotakis, and Emmanuel Stratakis**

The first reduction methodology, compatible with flexible, temperature-sensitive substrates, for the production of reduced spin-coated graphene oxide (GO) electrodes is reported. It is based on the use of a laser beam for the in situ, non-thermal, reduction of spin-coated GO films on flexible substrates over a large area. The photoreduction process is one-step, facile, and is rapidly carried out at room temperature in air without affecting the integrity of the graphene lattice or the flexibility of the underlying substrate. Conductive graphene films with a sheet resistance of as low as 700 Ω sq^{-1} and transmittance of 44% can be obtained, much higher than can be achieved for flexible layers reduced by chemical means. As a proof of concept of our technique, laser-reduced GO (LrGO) films are utilized as transparent electrodes in flexible, bulk heterojunction, organic photovoltaic (OPV) devices, replacing the traditional ITO. The devices displayed a power-conversion efficiency of 1.1%, which is the highest reported so far for OPV device incorporating reduced GO as the transparent electrode. The in situ non-thermal photoreduction of spin-coated GO films creates a new way to produce flexible functional graphene electrodes for a variety of electronic applications in a process that carries substantial promise for industrial implementation.

1. Introduction

Transparent and flexible electronics have been of great interest due to their attractive applications in displays, e-paper, touch panels and photovoltaics.[1] In addition to being electrically conductive and optically transparent, electrode materials of next-generation flexible electronic devices are required to be robust under extensive bending and compatible with large-scale manufacturing.[2] Indium tin oxide (ITO) is the currently leading transparent conductive electrode in rigid optoelectronic devices.[3] However, ITO cannot fulfill such requirements, since it is brittle and cracks under bending or stretching,[4] and on top of that it is practically expensive, since it suffers from both the indium scarcity and the sputter deposition line expenses.[5] Furthermore, device issues like instability of ITO toward acidic or basic conditions[6] and mechanical brittleness[7] limit the applicability of ITO in flexible electronics. A flexible substitutive material for ITO with a similar performance but lower cost is evidently needed. Recent research has focused on the development of thin layers of highly transparent conductive films based among, other materials, on solution-processed carbon nanotubes (CNTs), metal gratings, and random networks of metallic nanowires.[8–13] These materials appear to be attractive alternatives for applications requiring low-cost large-area fabrications and flexibility; however, they exhibit relatively high roughness, reducing the reproducibility rate of the devices.

The experimental discovery of graphene brought a new alternative to commercially available ITO electrodes. Graphene is a single atomic monolayer of sp^2-bonded carbon atoms.[14] As a zero band-gap semiconductor, the electrons delocalize over the complete sheet, which provides ballistic charge transport in a one-atom-thick material with very little optical absorption.[15] Solution-based graphene has been identified as a potential replacement for ITO in flexible electronics,[16–18] since it is highly conductive, transparent, bendable, and air- and high-temperature-stable, while it offers the possibility of deposition on large area and flexible substrates, compatible with roll-to-roll manufacturing methods.[19,20] Moreover, the graphene films exhibit a higher transmittance over a wider wavelength range than CNTs[21] and ITO.[22] Although research is still at its early stages, the excellent performance of various graphene-based electronic devices gives graphene a realistic chance of being competitive in transparent and bendable technologies, compared with traditional transparent electrodes.[23] Recently, the concept of using graphene as the transparent conductive electrode in organic photovoltaics (OPVs) has been realized by several groups.[24–27]

Prof. E. Kymakis, M. M. Stylianakis
Center of Materials Technology and Photonics
& Electrical Engineering Department
Technological Educational Institute (TEI) of Crete
Heraklion 71004 Crete, Greece
E-mail: kymakis@staff.teicrete.gr
K. Savva, Prof. C. Fotakis, Dr. E. Stratakis
Institute of Electronic Structure and Laser (IESL)
Foundation for Research and Technology-Hellas (FORTH)
Heraklion, 71110 Crete, Greece
E-mail: stratak@iesl.forth.gr
K. Savva, Prof. C. Fotakis
Department of Physics
University of Crete
Heraklion, 71003 Crete, Greece
M. M. Stylianakis
Department of Chemistry
University of Crete, Heraklion, 71003 Crete, Greece
Dr. E. Stratakis
Department of Materials Science and Technology
University of Crete
Heraklion, 71003 Crete, Greece

DOI: 10.1002/adfm.201202713

Furthermore, solution-processed graphene-based materials have been utilized as the electron-acceptor material in OPVs.[28–30]

To date, the most eye-catching method for preparing graphene electrode films over large and flexible areas is the solution processing of graphene oxide (GO), mainly due to the high-throughput preparation, low cost, and the simplicity of the fabrication technique. This method is based on solution-casting of GO, synthesized from inexpensive graphite powders onto a substrate, followed by reduction to graphene through chemical reaction with reducing agents and/or high-temperature annealing.[31–34] However, the GO-reduction methodologies are not compatible with flexible substrates, such as polyethylene terephthalate (PET), since PET cannot stand high temperature and typically melts at 250 °C; on the other hand, the deoxygenating processes are time-consuming and complicated. OPV devices with reduced graphene oxide electrodes (rGO) have been successfully realized on glass substrates by several processing and reduction methods, but all are incompatible with the PET substrates. For example, graphene electrodes were demonstrated by spin-coating or vacuum filtration of GO solution on glass, followed by reduction through exposure to hydrazine vapor and/or high-temperature annealing under vacuum or argon to render the material electrically conductive.[27,31,35,36] It is evident that the above approaches cannot be applied in PET substrates.

The only compatible method was most recently presented, where a flexible OPV device was fabricated by using a transferred rGO film as the transparent electrode.[37] But in this case, the GO is initially spin-coated in a SiO_2/Si substrate and therefore an additional processing step – transfer to the PET electrode – is required, resulting in high cost and complexity in the device fabrication. Furthermore there are issues concerning the efficiency of the transfer process for large areas. Therefore a low-cost high-throughput and facile method for making graphene electrodes without the need for high-temperature annealing is highly desirable. Most recently, several groups have demonstrated that GO solution can be reduced by a photo-irradiation process, such as UV-induced photocatalytic reduction,[38] photo-thermal reduction using a pulsed Xenon flash,[39] or selective laser reduction and patterning.[40–43] One of the advantages of laser-irradiating processes is that they do not rely on the use of chemicals or high temperatures, while the photoreaction time is shortened from several hours to a few minutes.[44]

In this paper, a novel facile and rapid methodology is presented to provide transparent and highly conductive graphene layers, produced by spin-casting on flexible substrates, to be used as electrodes for organic electronic applications. Such layers were realized through in situ pulsed-laser induced non-thermal reduction of spin-coated GO films on PET substrates. Although direct laser-writing techniques have been employed for the simultaneous reduction and patterning of GO layers,[40–43] the preparation of large-area flexible reduced-GO films has not been realized to date. As a proof of the success of our approach the fabricated layers were used as the transparent electrode in flexible poly-(3-hexylthiophene) (P3HT): phenyl-C61-butyric acid methyl ester (PCBM) photovoltaic devices and showed remarkable performance. The primary advantage of utilizing laser irradiation for the reduction of spin-coated GO films lies in the ability for in situ controlled epidermal treatment without practically affecting the integrity of the thermally sensitive substrate underneath. The GO reduction is manifested by a prominent increase of the sheet conductivity confirmed by a decrease in the oxygen level from ca. 61% in as-prepared GO down to ca. 17% for pulsed-laser-irradiated GO, while in the whole reduction process the PET substrate remained intact. The sheet resistance of the laser treated rGO (LrGO) electrodes was directly related to the power conversion efficiency of the respective OPV devices. The optimum LrGO electrodes were found to exhibit a thickness of ca. 20 nm, a sheet resistance of 2 kΩ sq^{-1} and a transparency of more than 70% over the 400–1100 nm spectral range.

2. Results and Discussion

Figure 1a presents the irradiation scheme used for the preparation of the LrGO electrodes. The as-spun GO layers on PET were subjected to irradiation by a femtosecond (fs) laser beam

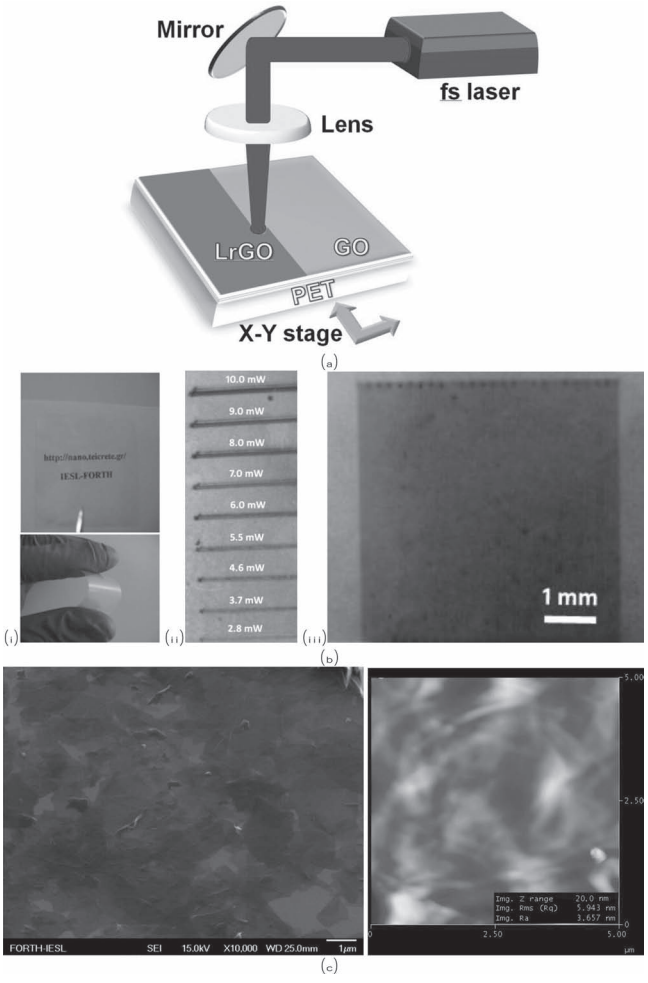

Figure 1. a) Schematic of the experimental technique used for the reduction of GO films on PET substrates. b) Typical photos of: i) flexible GO films, ii) scan lines obtained upon irradiation with 100 fs pulses at different fluences indicating the gradual color change due to reduction, and, iii) large processed area; the black spots inside the irradiated area correspond to regions where the GO material is ablated. c) SEM and AFM images of LrGO films on PET.

that was translated onto the film area. The detailed process is given in the Experimental Section. Due to the ultrashort pulse duration, selective removal of the oxygen groups on GO sheets takes place in air without any ablation occurring. By carefully tuning key laser parameters, the reduction degree of GO could be controlled in the irradiated region. For example, Figure 1b-ii shows scan lines and the corresponding coloration changes induced in a flexible GO film (Figure 1b-i) surface after the laser-assisted reduction process at various incident irradiation powers. The yellowish color of the pristine film was gradually turned into black with the elevation of laser fluence, indicating that GO is rapidly reduced by pulsed-laser irradiation. For the preparation of the LrGO electrodes, the entire film area was scanned by overlapping repetitive single scan laser lines (Figure 1b-iii). SEM and AFM analysis performed on the irradiated areas confirm that the film roughness is not practically affected by the laser treatment process, except from localized spots corresponding to locations with lower ablation threshold (**Figure 2**b). However, heating effects during the laser reduction process that deform the PET/GO interface may also be the cause of the appearance of such spots.

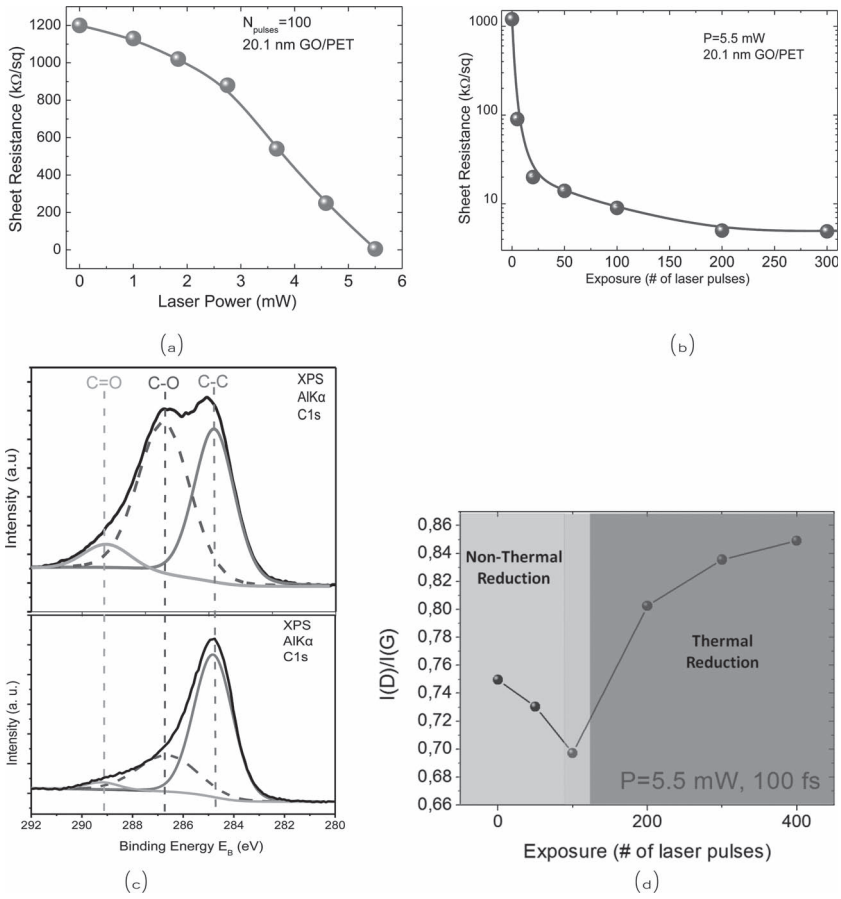

Figure 2. Dependence of sheet resistance of a LrGO film on: a) the fs laser output power, and, b) the number of fs pulses per irradiating spot. c) XPS spectra on the pristine (top) and fs laser-treated GO areas (bottom) at 5.5 mW per 100 pulses per spot. d) Dependence of the D/G peaks intensity ratio on the number of fs pulses per irradiating spot.

The utility of graphene films in applications as transparent electrodes in OPVs is governed by the sheet resistance and visible-light transmission. Either of these properties can be individually tuned to the desired value by changing the graphene electrode thickness and the respective degree of reduction. In our technique, by carefully tuning key laser parameters, the reduction degree of GO could be readily controlled. The results presented here, regarding the optical and electronic performances of the LrGO films, correspond to the best conductive films attained through optimum tuning of the laser treatment parameters for the various film thicknesses tested. In particular, the laser output power strongly affects the sheet resistance of the LrGO films and, as shown in Figure 2a, the conductivity increases by more than two orders of magnitude with a small increase of the laser power. When the incident power exceeds 5.5 mW the GO layers were partly ablated, while the film roughness becomes more pronounced (Supporting Information Figure S1). Furthermore, for constant incident power the film resistivity decreases upon increasing the average number of pulses per spot, *N*, until saturation is reached for high pulse numbers (Figure 2b). It is evident that a more than three orders of magnitude decrease in sheet resistance can be realized via proper selection of laser energy and number of pulses. Notably, as confirmed by SEM imaging, the morphology of irradiated area was not significantly altered through this process. This optimal resistivity change is due to a significant reduction of the GO sheets, as evidenced by XPS measurements, shown in Figure 2c. Indeed, the carbon content bonded to oxygen is reduced from 61% in the initial GO to 16% in LrGO, indicating that the majority of oxygen groups were removed. It should be emphasized that such improvement can be achieved without any apparent damage in the mechanical properties and integrity of the PET substrate.

Raman spectra recorded from pristine and irradiated regions (Supporting Information Figure S4) showed that the characteristic broad peaks at 1354, 1580, and 2695 cm^{-1}, corresponding to D, G, and 2D bands, respectively, become sharper after laser treatment. In addition, there is no significant band shift and broadening. To account for the crystalline quality of the LrGO sheets, the D/G intensity ratio, which is a measure of the lattice disorder,[45] was monitored upon increasing the number of irradiation pulses at constant incident power (5.5 mW). As shown in Figure 2c, though the D/G intensity ratio of LrGO becomes slightly lower for low *N*, it significantly increases after prolonged irradiation with higher number of pulses. Therefore, for low *N*, a non-thermal ultrafast excitation and subsequent removal of oxygen groups takes place, while the lattice order is preserved. With the progression of laser irradiation, thermal effects become more and more pronounced[46] giving rise to photothermal breakage of carbon bonds, which increases the

number of defects in the lattice and in turn leads to the formation of smaller and smaller crystalline graphene domains.[47] It is concluded that removal of oxygen atoms from graphene sheets takes place without causing any damage to the lattice by precise tuning of the laser power and pulse number, which is consistent with recent theoretical calculations.[48] The presence of non-thermal and thermal components during the reduction process is further supported by two additional experimental findings: a) contrary to the fs case, the D/G peak intensity is rapidly and monotonically increasing upon irradiation with nanosecond (ns) laser pulses of the same incident fluence (Supporting Information Figure S5); and, b) the ablation threshold was shifted to lower fluences when the pulse repetition rate is increased from kHz to MHz (Supporting Information Figure S6) indicating cumulative effects due to successive pulses. Therefore the mechanism of the oxygen removal can be attributed to electronic excitation non-thermal effect and the electron–hole (e–h) recombination-induced thermal effect. The former is significant in the first hundreds of femtoseconds, where electrons are excited from bonding to antibonding states and significantly weaken C–O electronic bonding near the top of the valence band, leading to an immediate oxygen removal. Upon excitation with ns pulses e–h recombination occurs during the pulse and heat reduction of GO dominates. It should be noted that the threshold fluence required to reduce the sheet resistance in our experiments, 3.5 mJ cm^{-2} (corresponding to 1 mW output power), is close to the recently predicted theoretical value for non-thermal removal of oxygen atoms from the GO lattice.[48]

Figure 3a shows the sheet resistance (R_{SH}) and the transmittance (T_R) at $\lambda = 550$ nm of LrGO films of different thicknesses. It is clear that both R_{SH} and T_R decreased upon increasing the graphene film thickness. The obtained lowest R_{SH} is 0.7 kΩ sq^{-1} for the 20.1 nm thick LrGO film, the transmittance of which is 44%. The highest optical transparency of 88% was obtained for the 4.5 nm thick LrGO, but the sheet resistance is 18 kΩ sq^{-1}. These results are similar to the previous reports of flexible graphene films fabricated by chemically reduced GO films[49,37] transferred onto PET substrates. Another advantage of the LrGO electrodes on PET is the possibility of application in flexible electronic devices. Figure 3b shows the averaged sheet resistance of the LrGO films with various thicknesses, normalized with the R_{SH} before bending, under different bending angles, which are defined as the angles of intersections drawn from two bent ends. The inset shows the sheet resistance of the same films of the Figure 3b as a function of the bending angle. The change in the sheet resistance becomes appreciable after 90°, while, the overall change is less than 13% up to 135°. This implies that no appreciable cracks occur in the film during bending. This excellent flexibility is advantageous over the conventional ITO, which shows a rapid increase in the sheet resistance due to cracking of the film as the bending angle increases, and experiences a catastrophic electrical failure (reduction of conductivity by three orders of magnitude) at a bending angle around 50°–60°.[50,51]

The next step is to fabricate OPV devices on the top of the LrGO films in order to determine their photovoltaic characteristics and identify the combination of transparency and resistance that provides the best performance. The OPV device works as in

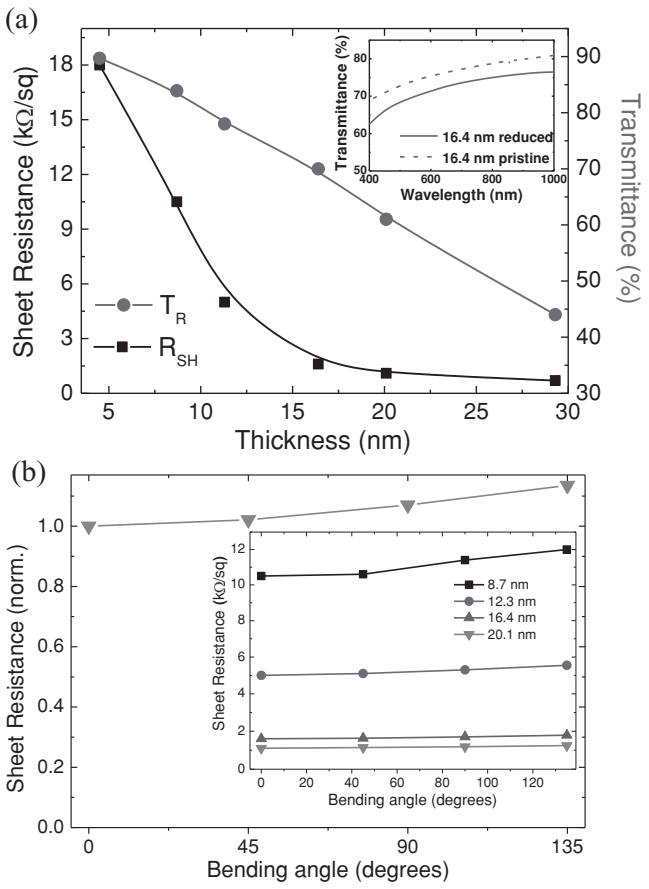

Figure 3. a) Transmittance at 550 nm and sheet resistance of the LrGO films on PET substrates as a function of their film thickness. The inset shows the UV-vis transmittance spectra of the LrGO films on PET. b) Sheet resistance vs bending cycles of flexible CVD graphene films. The sheet resistance has been normalized with the sheet resistance measured before bending.

the case of traditional P3HT:PCBM device; the photogenerated excitons are dissociated at the P3HT/PCBM interfaces at the active layer, with holes collected to the LrGO electrode through the hole transport layer, and electrons are collected at the top Al electrode. **Figure 4**c presents the illuminated *J–V* characteristics of the OPV devices with LrGO thicknesses of 4.6, 11.3, 16.4, and 20.1 nm. Their photovoltaic performance is summarized in **Table 1**.

The V_{OC} is constant at 0.57 V, and a variation is only observed for the device with the lowest LrGO thickness. This behavior is consistent, since V_{OC} is mainly governed by the energy levels offset between the highest occupied molecular orbital of P3HT and lowest unoccupied molecular orbital of PCBM.[52] Both photocurrent and fill factor increase with increasing LrGO thickness, due to the reduction of the sheet resistance of the LrGO films. The optimum thickness is about 16.4 nm, where a J_{SC} of 5.62 mA cm^{-2}, a V_{OC} of 0.57 V, a FF of 0.34, and an overall efficiency (η) of 1.1% were obtained. This value is the highest observed so far for flexible OPVs with reduced GO film, indicating the effectiveness of the laser ablation reduction method. In the case of GO reduction by thermal annealing

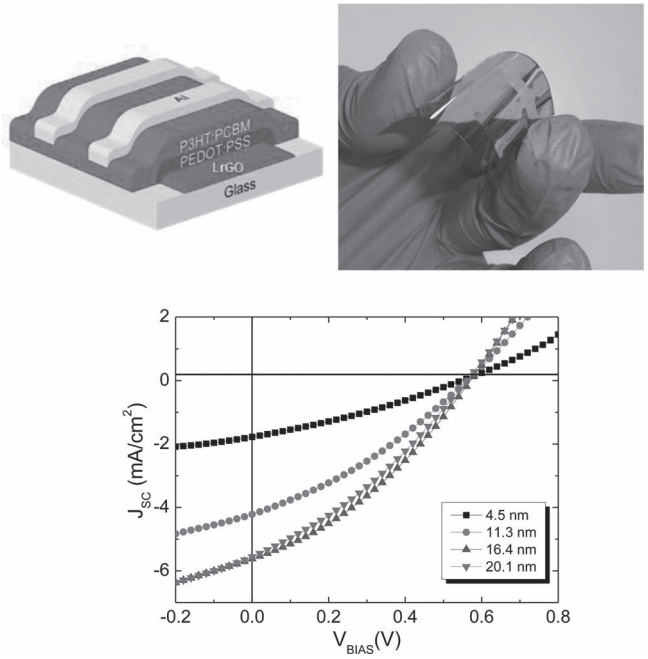

Figure 4. top) Schematic and picture of the flexible PET/rGO/PEDOT:PSS/P3HT:PCBM/Al photovoltaic devices fabricated; and, bottom) The illuminated current–voltage (*J–V*) curves of the solar cells with various LrGO film thicknesses.

in Ar/H_2 at 1000 °C, the best photovoltaic performance (η = 0.78%) was achieved with a 16 nm thick LrGO film having R_{SH} of 3.2 kΩ sq^{-1}, and T_R of 65%.[37] In our approach, where the reduction takes place by laser ablation, an efficiency enhancement by 41% is obtained with a 16.4 nm thick film having R_{SH} of 1.6 kΩ sq^{-1}, and T_R of 70%. Therefore, it is evident that the higher conductivity of the LrGO film is responsible for the higher efficiency, indicating the superiority of the laser ablation method, compared with the chemical one. Furthermore, the reduction process takes place in situ on the flexible spin-cast GO film, which is not the case in all other relevant work.

One of the motivations using solution-cast LrGO electrodes is to realize highly flexible OPVs that can be used for compact roll-type solar modules. **Figure 5** presents the results of an experiment monitoring the photovoltaic performance of flexible OPVs as a function of the bending angle. As can be seen, the photovoltaic characteristics are slightly degraded upon bending,

Table 1. Photovoltaic performance of the solar cells incorporating LrGO electrodes.

GO thickness [nm]	J_{SC} [mA cm^{-2}]	V_{OC} [V]	FF	η [%]
4.6	1.77	0.55	0.3	0.29
11.3	4.22	0.57	0.32	0.76
16.4	5.62	0.57	0.34	1.1
20.1	5.56	0.57	0.32	1.01

and are still functional even for bending angles up to 135°. In contrast, the traditional ITO (Sigma Aldrich, R_{SH} = 100 Ω sq^{-1}) OPV devices operate only for bending up to 45°, and fail completely at 65°. For the LrGO devices, as the bending angle increases, both the J_{SC} and FF decay, while V_{OC} remains constant. This decay can be directly related to the decreased sheet resistance during bending, as shown in Figure 5. Since the FF parameter highly depends on the LrGO electrode properties, the dependence of the FF on the bending angle clearly demonstrates the superiority of the LrGo electrodes over the ITO electrodes in terms of flexibility.

A theoretical simulation was carried out to provide an insight into the heat absorption and subsequent thermal effect on the temperature sensitive PET substrate during laser reduction the GO film. To account for the maximum laser heating effect attained the simulation is performed in the case of irradiation with ns laser pulses of the same fluence (17.5 mJ cm^{-2}) as that used for the fs reduction process (Supporting Information Figure S5). In this case, the dynamics of laser heating can be considered as a typical three-dimensional heat-flow problem, which can be simulated by the solution of the heat conduction equation:[53]

$$\rho C_p \frac{\partial T(r,t)}{\partial t} - \frac{\partial}{\partial x}\left(\frac{\partial T(x,t)}{\partial x}\right) - \frac{\partial}{\partial y}\left(k\frac{\partial T(y,t)}{\partial y}\right) - \frac{\partial}{\partial z}\left(k\frac{\partial T(z,t)}{\partial z}\right) = S(x,y,z) \quad (1)$$

where ρ is the mass density, C_p is the specific heat, k is the thermal conductivity, and $S = \alpha I(x,y,z,t)$ is an internal heat source, with α being the absorption coefficient. The x, y directions lie in the film plane while z corresponds to the direction perpendicular to the film surface. The laser power density I has a Gaussian profile and can be considered to have a temporal and spatial part with an exponential decay and is written as:[44]

$$I(x, y, z, t) = 0.94(1 - R) I_o(x, y) \exp(-\alpha z) \exp\left[-4 \ln 2 \left(\frac{t}{t_p}\right)^2\right] \quad (2)$$

with

$$I_o(x, y) = \frac{J}{t_p} \exp\left[-\frac{x^2 + y^2}{r_g^2}\right] \quad (3)$$

where R is the GO film reflectivity, J is the laser fluence, t_p is the pulse duration (i.e., full-width-at-half-maximum), and r_g is the radius of the Gaussian beam.

A finite element model (FEM) is used to calculate the temperature distribution around the spot center following irradiation of a 20.1 nm thin GO film on PET with 100 pulses of 20 ns at a fluence of 17.5 mJ cm^{-2}. Details of the FEM method can be found in the Supporting Information. **Figure 6** presents the simulated temperature profile within a cross-sectional area of the GO/PET system and the corresponding temperature variation as a function of the depth from the GO film surface (z = 0). The highest attainable temperature is below 350 °C indicating that the laser heating might induce removal of oxygen functional groups, considering that the desorption of such groups from GO occurs around 200–230 °C.[54] During this reduction

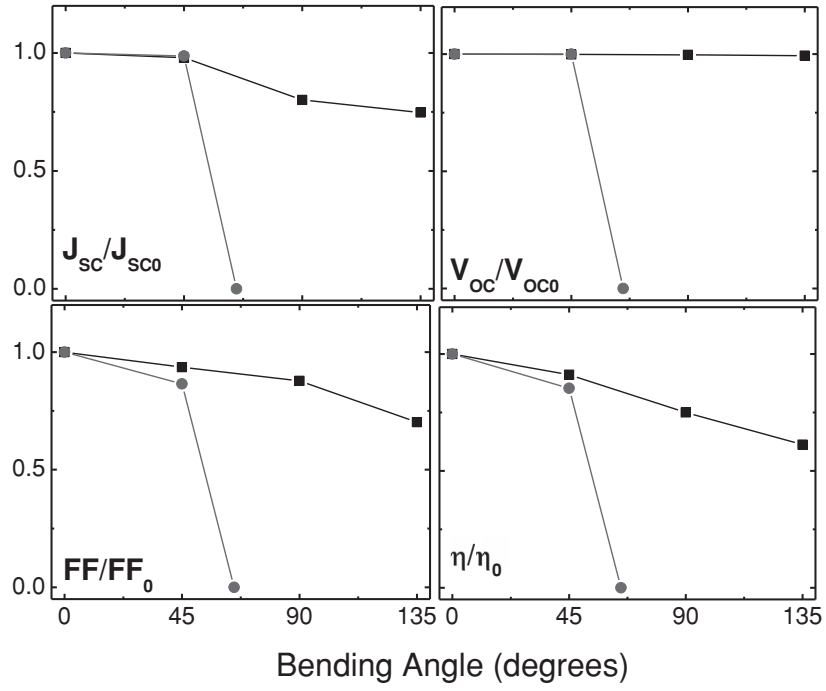

Figure 5. Evolution of photovoltaic parameters of LrGO (squares) and ITO (circles) based OPV devices under bending at different angles.

process the PET substrate is slightly affected since, as shown in Figure 6, a ca. 3 μm layer, corresponding to ca. 3.5% of its total thickness, is estimated to exceed its melting point. In case of fs laser treatment the pulse duration is comparable with the electron–phonon thermalization time and therefore during the pulse electrons and lattice are out of local thermal equilibrium. Such non-equilibrium heating process should be modeled in two steps, first the absorption of photon energy by electrons and then heating of the lattice via electron–phonon coupling. In the particular case of fs laser irradiation of a nanometric film on a substrate under sub-ablation conditions considered here, theoretical and experimental investigations indicate that the heating effects are much less pronounced compared to the longer pulse irradiation due to the absence of electron–phonon coupling during the pulse; under such conditions non-thermal excitation effects become dominant.[55,56] Therefore it is expected that the maximum attainable temperatures will be much lower than those calculated in Figure 6 for the extreme case of ns irradiation. This in turn supports our experimental evidence for non-thermal reduction of GO achieved upon irradiation with fs pulses. It should be noted here that it is difficult to perform simulations for the fs case, considering that some of the constants required for the calculation, i.e., electron and lattice specific heats, electron relaxation time, and electron–phonon coupling factor, have not yet been reported in the literature.

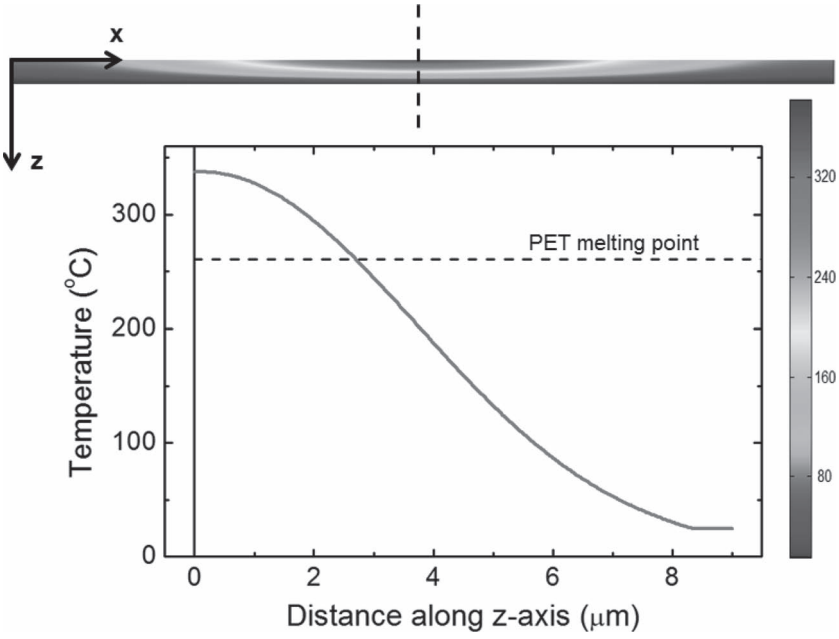

Figure 6. Thermal modelling results: top) cross-sectional contour plot showing the temperature distribution within a 320 μm × 9 μm area of the GO/PET system; and, bottom) temperature gradient along *z*- axis (the surface of GO film corresponds to $z = 0$); the dashed line indicates the melting temperature of PET.

3. Conclusions

We have demonstrated an efficient laser-based reduction method for fabricating flexible conductive and transparent graphene films that were spin-cast on temperature-sensitive substrates. This technique is particularly attractive considering that it is applied in situ in one step and does not require additional transfer of the reduced film to the flexible substrate. Furthermroe, compared to chemical and high-temperature thermal methods, pulsed-laser photoreduction is simplified, rapid, energy efficient, and poisonous material-free. It is shown that the LrGO films can be effectively integrated in polymer–fullerene photovoltaic cells, as the transparent electrode, replacing ITO. This application requires graphene films as transparent and conductive as possible, a property that cannot be easily obtained since there is a trade-off between these two requirements. Nevertheless, photovoltaic characteristics with an efficiency of 1.1% are obtained with a LrGO film with 70% transparency and sheet resistance of 1.6 kΩ sq^{-1}. Towards improving

film conductivity, the high degree of flexibility offered by different combination of irradiation parameters, may enable the production of LrGO films with even lower resistance, without lowering the transparency.

The advantages of this approach include a cost-effective, simple solution process using graphene, which makes LrGO electrodes versatile for applications not only in OPVs described in this work, but also in other optoelectronic devices, such as flat-panel displays, and organic light-emitting devices. By employing the optical schemes and translation systems that have already been developed for industrial lasers, rapid large-area processing can be realized that makes this technique easily adaptable to a roll-to-roll manufacturing line.

4. Experimental Section

Preparation of GO Films: GO was prepared from purified natural graphite powder (Alfa Aesar) according to a modified Hummers' method.[57,58] Specifically, graphite powder (0.5 g) was placed into a cold mixture of concentrated H_2SO_4 (40 mL, 98%) and $NaNO_3$ (0.375 g) under vigorous stirring for 1 h, in an ice bath. During this time $KMnO_4$ (2.25 g) was added in portions and the mixture kept in the ice bath for a further 2 h, in order to cool the mixture to under 10 °C. The green–brown colored mixture was stirred for 5 d. On completion of the reaction, the brick-colored mixture was mixed with an aqueous solution of 5% H_2SO_4 (70 mL). The mixture was stirred for 1 h under heating at 98 °C and became grey–black colored. When the temperature was decreased to 60 °C, 30% H_2O_2 (ca. 2 mL) was added and the mixture stirred for 2 h at room temperature. In order to remove acidic ions, especially these of Mn, we used the following process. The mixture was centrifuged for 5 min at 4200 rpm and washed with ca. 600 mL of an aqueous solution of 3% H_2SO_4 (ca. 9 mL)/0.5% H_2O_2 (ca. 1.5 mL) and then put in an ultrasonic vibration bath for 10 min (the ultrasonic vibration exfoliates the graphite oxide to GO sheets). The process was repeated ten times. Then, the mixture was washed and purified with 150 mL of aqueous solution 3% HCl (ca. 1.5 mL) three times. Afterwards, it was washed thoroughly with distilled water (1D) and acetone, in order to remove any remaining acidicity. Finally the material was dried to obtain a loose brown powder, which can be stored indefinitely.[21]

For the preparation of the electrodes, flexible PET (Goodfellow) pieces (15 mm × 15 mm) with 90 µm thickness were used as substrates. PET substrates were cleaned by detergent followed by ethanol and Milli-Q water and subsequently treated by O_2 plasma to provide a more hydrophilic surface. For the preparation of the thin films, 15 mg mL^{-1} GO solution in ethanol was spin-coated at 1000 rpm onto the PET substrates. The initial volume of the GO solution was used as a means to control the thickness of spin-coated GO films. Following the spin-coating process, the GO films were dried at 70 °C inside a nitrogen-filled glove box. For the experiments, a series of films were produced; their thicknesses were measured using profilometer (Veeco) measuring the height profile of steps formed between covered and uncovered substrate areas. The root-mean-square (rms) roughness determined from 3 × 3 μm^2 AFM scan areas varied from 3–5 nm. The sheet resistance was measured in a four-electrode configuration and includes the contact resistance between the graphene film and thermally evaporated gold electrodes used to probe the films.

Pulsed-Laser Reduction: The pulsed-laser reduction system consists of a Ti:Sapphire (Tsunami, Spectra-Physics) laser (λ = 800 nm) delivering 100 fs pulses at a repetition rate of 1 kHz. The laser beam was focused down to 170 µm onto the GO film using a 10 mm lens. For the experiments, the laser output power was varied in the range of 1.0–10 mW corresponding to fluences of 3.5–35 mJ cm^{-2}. GO films were mounted on a high-precision *X*–*Y* translation stage normal to the incident laser beam. A mechanical shutter was synchronized to the stage motion to provide for a uniform exposure of the sample area to a constant number of pulses. In order investigate the repetition rate effect on the reduction process, pulses from a fs laser oscillator of 800 nm, 100 fs pulse duration, and 80 MHz repetition rate were used. In order to investigate the effect of pulse duration, pulses from a KrF excimer laser of 248 nm, 30ns pulse duration, and 10 Hz repetition rate were used. In all cases the range of fluences used was the same. Prior to OPV device fabrication, the laser treated rGO/PET electrodes were cleaned by Milli-Q water and baked at 150 °C for 2 h.

Microscopic and Spectroscopic Characterization: The samples were characterized by Raman spectroscopy at room temperature on a Nicolet Almega XR Raman spectrometer (Thermo Scientific) with a 473 nm blue laser as an excitation source. UV-vis absorption spectra were recorded using a Shimadzu UV-2401 PC spectrophotometer over the wavelength range of 400–1000 nm. The morphology of the surfaces was examined by field emission scanning electron microscopy (FE-SEM; JEOL JSM-7000F) and by atomic force microscopy (AFM; Digital Instruments NanoScope IIIa).

Fabrication and Characterization of Photovoltaic Devices: The prepared rGOs on PET substrates were further treated with O_2 plasma to generate the hydrophilic surface of rGO. PEDOT:PSS films (VP AI 4083) were filtered through a 0.45 µm PVDF filter and spin-coated on the rGO films at 4000 rpm for 30 s followed by a 10 min annealing at 100 °C inside a nitrogen filled glove box. The photoactive layer, consisting of P3HT (Rieke Metals) and PCBM (Nano-C) dissolved in 1,2-dichlorobenzene (DCB), was spin-coated on top of the HTL layer. Equal volume solutions of P3HT from Rieke Metals (34 mg mL^{-1}) and PCBM from Nano-C (34 mg mL^{-1}) were prepared in dichlorobenzene and stirred for 2 h at 40 °C, and filtered with a 0.2 µm PTFE filter. The P3HT:PCBM photoactive layer was spin-coated on top of the PEDOT:PSS layer. The wet film was then transferred to a Petri dish and subjected to solvent annealing. Devices were completed by the thermal evaporation of 40 nm of aluminium forming a device area of 0.18 cm^2. A post fabrication annealing was performed at 150 °C for 5 min in nitrogen. Current–voltage (*J*–*V*) measurements were performed at room temperature using an Agilent B1500A Semiconductor Device Analyzer. For photovoltaic characterization the cells were illuminated with 100 mW cm^{-2} power intensity of white light by an Oriel solar simulator with an AM1.5 filter through the glass/ITO side. All measurements were made in air immediately after device fabrication. The optical transmission properties of the graphene were recorded with a UV–visible spectrophotometer (Shimadzu). The measurements of surface resistivity were carried using the four-probe technique (Ecopia HMS) using gold contacts. The thickness of the prepared films was estimated by a profilometer (Veeco) measuring the height profile of steps formed between covered and uncovered substrate areas.

Supporting Information

Supporting Information is available from the Wiley Online Library or from the author.

Acknowledgements

This work was supported by the Integrated Initiative of European Laser Research Infrastructures LASERLAB-II (Grant Agreement No. 228334). The authors acknowledge Dr. G. Konstantinidis of the Microelectronics Research group of FORTH for the profilometry measurements.

Received: September 18, 2012
Revised: November 26, 2012
Published online: January 9, 2013

[1] W. J. Yu, S. H. Chae, S. Y. Lee, D. L. Duong, Y. H. Lee, *Nano Lett.* **2011**, *11*, 1344–1350.
[2] A. Kumar, C. Zhou, *ACS Nano* **2010**, *4*, 11–14.

[3] S. H. Park, A. Roy, S. Beaupre, S. Cho, N. Coates, J. S. Moon, D. Moses, M. Leclerc, K. Lee, A. J. Heeger, **2009**, *3*, 297–302.
[4] D. S. Hecht, L. Hu, G. Irvin, *Adv. Mater.* **2011**, *23*, 1482–1513.
[5] B. A. Andersson, *Prog. Photovolt. Res. Appl.* **2000**, *8*, 61–76.
[6] S. R. Forrest, *Nature* **2004**, *428*, 911–918.
[7] B. Paci, A. Generosi, Bailo, D. V. Rossi Albertini, R. De Bettignies, *Chem. Phys. Lett.* **2010**, *494*, 69–74.
[8] Z. C. Wu, Z. H. Chen, X. Du, J. M. Logan, J. Sippel, M. Nikolou, K. Kamaras, J. R. Reynolds, D. B. Tanner, A. F. Hebard, A. G. Rinzler, *Science* **2004**, *305*, 1273–1276.
[9] L. Hu, D. S. Hecht, G. Grüner, *Nano Lett.* **2004**, *4*, 2513–2517.
[10] E. Kymakis, E. Stratakis, E. Koudoumas, *Thin Solid Films* **2007**, *515*, 8598–8600.
[11] J.-Y. Lee, S. T. Connor, Y. Cui, P. Peumans, *Nano Lett.* **2008**, *8*, 689–692.
[12] E. Kymakis, E. Stratakis, E. Koudoumas, C. Fotakis, *IEEE Trans. Electron Devices* **2011**, *58*, 860–864.
[13] S. Kim, Y. Yim, X. Wang, D. D. C. Bradley, S. Lee, J. C. DeMello, *Adv. Funct. Mater.* **2010**, *20*, 2310–2316.
[14] A. K. Geim, K. S. Novoselov, *Nat. Mater.* **2007**, *6*, 183–191.
[15] M. Hirata, T. Gotou, S. Horiuchi, M. Fujiwara, M. Ohba, *Carbon* **2004**, *42*, 2929–2937.
[16] F. Bonaccorso, Z. Sun, T. Hasan, A. C. Ferrari, *Nat. Photonics* **2010**, *4*, 611–622.
[17] Z. Y. Yin, S. X. Wu, X. Z. Zhou, X. Huang, Q. C. Zhang, F. Boey, H. Zhang, *Small* **2010**, *6*, 307–312.
[18] X. Huang, Z. Zeng, Z. Fan, J. Liu, H. Zhang, *Adv. Mater.* **2012**, DOI: 10.1002/adma.201201587.
[19] K. S. Kim, Y. Zhao, H. Jang, S. Y. Lee, J. M. Kim, K. S. Kim, J. H. Ahn, P. Kim, J. Y. Choi, B. H. Hong, *Nature* **2009**, *457*, 706–710.
[20] H. A. Becerril, J. Mao, Z. Liu, R. M. Stoltenberg, Z. Bao, Y. Chem, *ACS Nano* **2008**, *2*, 463–470.
[21] S. De, J. N. Coleman, *ACS Nano* **2010**, *4*, 2713–2720.
[22] T. Minami, *Sci. Technol.* **2005**, *20*, S35.
[23] S. Bae, H. Kim, Y. Lee, X. F. Xu, J. S. Park, Y. Zheng, J. Balakrishnan, T. Lei, H. R. Kim, Y. I. Song, Y. J. Kim, K. S. Kim, B. Ozyilmaz, J. H. Ahn, B. H. Hong, S. Iijima, *Nat. Nanotechnol.* **2010**, *5*, 574–578.
[24] Y. Wang, X. H. Chen, Y. L. Zhong, F. R. Zhu, K. P. Loh, *Appl. Phys. Lett.* **2009**, *95*, 063302.
[25] G. Eda, Y. Y. Lin, S. Miller, C. W. Chen, W. F. Su, M. Chhowalla, *Appl. Phys. Lett.* **2008**, *92*, 233305.
[26] J. Wu, H. A. Becerril, Z. Bao, Z. Liu, Y. Chen, P. Peumans, *Appl. Phys. Lett.* **2008**, *92*, 263302.
[27] L. G. D. Arco, Y. Zhang, C. W. Schlenker, K. Ryu, M. E. Thompson, C. Zhou, *ACS Nano* **2010**, *4*, 2865–2873.
[28] Q. Liu, Z. F. Liu, X. Y. Zhang, L. Yang, N. Zhang, G. P. Pan, S. G. Yin, Y. Chen, *Adv. Funct. Mater.* **2009**, *19*, 894–904.
[29] M. M. Stylianakis, E. Stratakis, E. Koudoumas, E. Kymakis, S. H. Anastasiadis, *ACS Appl. Mater. Interfaces* **2012**, *4*, 4864–4870.
[30] M. M. Stylianakis, G. D. Spyropoulos, E. Stratakis, E. Kymakis, *Carbon* **2012**, *50*, 5554–5561.
[31] V. C. Tung, M. J. Allen, Y. Yang, R. B. Kaner, *Nat. Nanotechnol.* **2008**, *4*, 25–29.
[32] G. Eda, G. Fanchini, M. Chhowalla, *Nat. Nanotechnol.* **2008**, *3*, 270–274.
[33] X. Huang, X. Y. Qi, F. Boey, H. Zhang, *Chem. Soc. Rev.* **2012**, *41*, 666–686.
[34] X. Huang, Z. Y. Yin, S. X. Wu, X. Y. Qi, Q. Y. He, Q. C. Zhang, Q. Y. Yan, F. Boey, H. Zhang, *Small* **2011**, *7*, 1876–1902.
[35] Y. F. Xu, G. K. Long, L. Huang, Y. Huang, X. J. Wan, Y. F. Ma, Y. S. Chen, *Carbon* **2010**, *48*, 3308–3311.
[36] E. Kymakis, E. Stratakis, M. M. Stylianakis, E. Koudoumas, C. Fotakis, *Thin Solid Films* **2011**, *520*, 1238–1241.
[37] Z. Y. Yin, S. Y. Sun, T. Salim, S. X. Wu, X. Huang, Q. Y. He, Y. M. Lam, H. Zhang, *ACS Nano* **2010**, *4*, 5263–5268.
[38] G. Williams, B. Seger, P. V. Kamat, *ACS Nano*, **2008**, *2*, 1487–1491.
[39] L. J. Cote, R. C. Silva, J. X. Huang, *J. Am. Chem. Soc.* **2009**, *131*, 11027–11032.
[40] Y. Zhou, Q. L. Bao, B. Varghese, L. A. L. Tang, C. K. Tan, C. H. Sow, K. P. Loh, *Adv. Mater.* **2010**, *22*, 67–71.
[41] Y. L. Zhang, Q. D. Chen, H. Xia, H. B. Sun, *Nano Today* **2010**, *5*, 435–448.
[42] M. F. El-Kady, V. Strong, S. Dubin, R. B. Kaner, *Science* **2012**, *353*, 1326.
[43] W. Gao, N. Singh, L. Song, Z. Liu, A. L. M. Reddy, L. Ci, R. Vajtai, Q. Zhang, B. Wei, P. M. Ajayan, *Nat. Nanotechnol.* **2011**, *6*, 496.
[44] S. H. Ko, H. L. Pan, C. P. Grigoropoulos, C. K. Luscombe, J. M. J. Frechet, D. Poulikakos, *Nanotechnology* **2007**, *18*, 345202.
[45] L. M. Malard, M. A. Pimenta, G. Dresselhaus, M. S. Dresselhaus, *Phys. Rep.* **2009**, *473*, 51–87.
[46] B. N. Chichkov, C. Momma, S. Nolte, F. von Alvensleben, A. Tünnermann, *Appl. Phys. A* **1996**, *63*, 109–115.
[47] A. C. Ferrari, *Solid State Commun.* **2007**, *143*, 47–57.
[48] H. Zhang, Y. Miyamoto, *Phys. Rev. B* **2012**, *85*, 089901.
[49] H. Yamaguchi, G. Eda, C. Mattevi, H. Kim, M. Chhowalla, *ACS Nano* **2010**, *4*, 524–528.
[50] C. Biswas, Y. H. Lee, *Adv. Funct. Mater.* **2011**, *21*, 3806–3826.
[51] V. C. Tung, L. Chen, M. J. Allen, J. K. Wassei, K. Nelson, R. B. Kaner, Y. Yang, *Nano Lett.* **2009**, *9*, 1949–1955.
[52] E. D. Gomez, Y. L. Loo, *J. Mater. Chem.* **2010**, *20*, 6604–6611.
[53] H. Pan, D. H. Lee, S. H. Ko, C. P. Grigoropoulos, H. K. Park, T. Hoult, *Appl. Phys. A* **2011**, *104*, 29–38.
[54] Z. H. Liu, Z. M. Wang, X. Yang, K. Ooi, *Langmuir* **2002**, *18*, 4926.
[55] T. Q. Qiu, C. L. Tien, *J. Heat Transfer* **1993**, *115*, 842–847.
[56] H. D. Wang, W.-G. Ma, X. Zhang, W. Wang, Z. Y. Guo, *Int. J. Heat Mass Transfer* **2011**, *54*, 967–974.
[57] Z. Luo, Y. Lu, L. A. Somers, A. T. C. Johnson, *J. Am. Chem. Soc.* **2009**, *131*, 898–899.
[58] Z. B. Liu, Y. F. Xu, X. Y. Zhang, X. L. Zhang, Y. S. Chen, J. G. Tian, *J. Phys. Chem. B* **2009**, *113*, 9681–9686.